The oocyte zinc transporter *Slc39a10/Zip10* is a regulator of zinc sparks during fertilization in mice.

Atsuko Kageyama[1], Narumi Ogonuki[2], Takuya Wakai[3], Takafumi Namiki[1,4], Yui Kawata[1], Manabu Ozawa[5], Yasuhiro Yamada[6], Toshiyuki Fukada[7], Atsuo Ogura[2], Rafael A. Fissore[8], Naomi Kashiwazaki[1,9], Junya Ito[1,9,10*]

[1] Laboratory of Animal Reproduction, School of Veterinary Medicine, Azabu University, Sagamihara, 252-5201, Japan.

[2] Bioresource Engineering Division, Bioresource Research Center, RIKEN, Tsukuba, 305-0074, Japan.

[3] Department of Animal Science, Graduate School of Environmental and Life Science, Okayama University, Okayama, 700-8530, Japan.

[4] Present address: Department of Life Science Frontiers, Center for iPS Cell Research and Application (CiRA), Kyoto University, Kyoto, 606-8507, Japan.

[5] Laboratory of Reproductive Systems Biology, Center for Experimental Medicine and Systems Biology, The Institute of Medical Science, The University of Tokyo, Tokyo 108-8639, Japan.

[6] Department of Molecular Pathology, Graduate School of Medicine, The University of Tokyo, Tokyo 113-0033, Japan.

[7] Laboratory of Molecular and Cellular Physiology, Faculty of Pharmaceutical Sciences, Tokushima Bunri University, Tokushima 770-8514, Japan.

[8] Department of Veterinary and Animal Sciences, University of Massachusetts, Amherst 01003-9292, the United States.

[9] Graduate School of Veterinary Science, Azabu University, Sagamihara, 252-5201, Japan.

[10] Center for Human and Animal Symbiosis Science, Azabu University, Sagamihara, 252-5201, Japan.

*Correspondence:
Junya Ito, Laboratory of Animal Reproduction, Graduate School of Veterinary Sciences, Azabu University, Sagamihara, 252-5201, Japan, itoj@azabu-u.ac.jp

Abstract

In all vertebrates studied to date, a rise(s) in intracellular calcium is indispensable for successful fertilization and further embryonic development. Recent studies demonstrated that zinc is ejected to the extracellular milieu, the 'zinc spark', and follows the first few calcium rises of fertilization. However, the role of the zinc

sparks in fertilization and development, and the supporting influx mechanism(s) are unknown. In this study in mouse oocytes, we investigated the role of zinc transporters *Zip6/Slc39a6* and *Zip10/Slc39a10*. Zip10 mRNA or ZIP10 was expressed throughout folliculogenesis in oocyte or the plasma membrane, respectively. ZIP6 was also expressed in nuclear localization in oocytes and granulosa cells throughout folliculogenesis. The number of ovulated oocytes was examined in oocyte-specific *Zip6* (*Zip6*$^{d/d}$: *Zip6*$^{flox/flox}$ *Gdf9*$^{Cre/+}$) and *Zip10* (*Zip10*$^{d/d}$: *Zip10*$^{flox/flox}$ *Gdf9*$^{Cre/+}$) knockout mice, and no change was observed for either strain. *Zip10*$^{d/d}$ oocytes matured and formed normal metaphase II spindles, but had lower labile zinc levels as suggested by the zinc indicator, Fluozin-3 intensity. The levels of zinc fluorescence intensity in the *Zip6*$^{d/d}$ group were not different from the *Zip6*$^{f/f}$. Fertilization-induced calcium oscillations were present in both *Zip6*$^{d/d}$ and *Zip10*$^{d/d}$ oocytes, but zinc sparks were observed in *Zip6*$^{d/d}$ but not in *Zip10*$^{d/d}$ oocytes. Despite other events of egg activation proceeding normally in *Zip10*$^{d/d}$ oocytes, embryo development into blastocysts was compromised. We show here for the first time that the zinc transporter ZIP10 contributes to zinc homeostasis in oocytes and embryos, highlighting the pivotal role of this divalent cation in early development.

Classification

Major Classification: Biological Sciences

Minor Classification: Developmental Biology

Keyword: mammals, fertilization, zinc spark, embryo development, zinc signaling

Significance statement

Recent studies reported that the ejection of zinc into the extracellular milieu also called the 'zinc spark', occurs during mammalian fertilization including humans and all vertebrates. However, the role and molecules involved in producing these sparks remain unclear. We demonstrated for the first time that a zinc transporter, *Slc39a10/Zip10,* is required for the zinc sparks of fertilization in mice. In addition,

ZIP10-dependent zinc signaling is not involved in the zona reaction or the block of polyspermy but it is in embryonic development. Taken together, we show here a zinc transporter-dependent signaling event has pivotal roles in fertilization and embryonic development in mice. Our findings will contribute to improving embryonic development in all mammals.

Introduction

In mammalian fertilization, the sperm factor is released into the ooplasm to activate the oocyte (1). It is now believed that phospholipase C zeta (PLCζ) (1, 2) is the sperm factor and its induces in the ooplasm repetitive increases in the intracellular Ca^{2+}, termed 'calcium oscillations.' These oscillations play an essential role in triggering the oocyte activation events, such as cortical granule exocytosis, the block of polyspermy, meiotic resumption and exit from MII arrest (3-7). A calcium increase is highly conserved in many species as the trigger of egg activation and is vital for successful fertilization.

In recent years, zinc ions as well as calcium ions, are thought to play important roles during fertilization (8-10). Zinc ion is an essential trace element and the second most abundant transition ion in the human body after iron (11). Zinc homeostasis is essential for optimal metabolic function in the reproductive process in mammals (12), therefore zinc deficiency causes abnormalities such as fetal teratogenicity, long gestation periods, problematic labor, low birth weight and weak offspring (13, 14). Zinc also has important role in the male and female germ cells (9, 10). Especially in the mouse female germ cells, zinc-deficient condition caused profound defects in oocyte maturation, cumulus cell expansion and ovulation cycle (15). Several studies have been conducted in mice to understand how zinc regulates oocyte maturation. Zinc was reported to be a critical regulator of meiosis throughout oocyte maturation, including maintaining release from the first and second meiotic arrest (16). In addition, zinc levels of oocytes were found to increase by 50% as the oocyte progressed through meiosis (17, 18).

In 2011, Kim et al. reported the importance of zinc during mammalian fertilization (19). Zinc is predominantly stored in vesicles that are symmetrically

101 arranged along the oocyte cortex at the GV stage, and zinc-stored vesicles
102 (cortical granules) are located away from the spindle and form a hemispherical
103 pattern at the MII stage (19-24). After the penetration of sperm, it has been
104 induced a 'zinc spark' that releases billions of zinc ions from the cortical granules,
105 and the total zinc content of the oocytes decreases by 10-20% in at the end of
106 fertilization in mice (19, 25). In addition, these events immediately follow a series
107 of calcium oscillations (19). Zinc spark has also been observed in the cattle, non-
108 human primate, human and Xenopus laevis oocytes (19, 22, 26, 27), suggesting
109 that this phenomenon is a highly conserved event in vertebrate. More surprisingly,
110 full-term development of mouse embryos has been reported by chelation of Zn2+
111 ions without Ca2+ release, suggesting the depletion of zinc ions in oocytes may
112 be sufficient for oocyte activation. Zinc has also been reported to impact the
113 sperm during fertilization in mice. Zinc accumulation in the zona pellucida
114 increases fibril binding along the glycoprotein matrix and decreases the number
115 of sperm that can reach the fertilized oocytes (24, 28, 29). After the zinc sparks,
116 the released zinc affects the forward motility of sperm to prevent their passage
117 through the zona matrix (29). Zinc spark is associated with the release of
118 ovastacin (*Astl*, the official gene name), which is required for the zona reaction,
119 and functions as a polyspermy block mechanism that is initiated only a few
120 minutes after fertilization (29).

121 The transport of zinc ions into and out of cells is regulated by zinc
122 transporters. In mammals, 14 zinc ion importers, called as ZIP (ZIP1-ZIP14),
123 have been identified (30-32). Previous study showed that mammalian oocytes
124 regulate zinc uptake through two maternally derived and cortically distributed zinc
125 transporters, ZIP6 and ZIP10 (21). Further, they reported that targeted disruption
126 using *Zip6*- and *Zip10*- specific morpholino injection or antibody incubation
127 induced alteration of the intracellular labile zinc content, spontaneous resumption
128 of meiosis from the PI arrest and premature arrest at a telophase I-like state (21).
129 It is clear from these reports that ZIP6 and ZIP10 are involved in zinc transport in
130 oocytes, but the mechanisms are not clear. ZIP6 and ZIP10 form and function in
131 a complex (33), regulate glycogen synthase kinase (GSK-3) and other enzymes
132 in breast and kidney cancer cells, and regulate epithelial-mesenchymal transition

133 (EMT) (33, 34). ZIP10 is also involved in many life phenomena such as hair
134 follicles, skin epidermis and atopic dermatitis (35, 36). In addition, ZIP10 is also
135 an essential gene for embryonic hematopoiesis (37).
136 However, while functional analysis of the zinc transporters in various cells and
137 tissues has been conducted, the function of these zinc transporters in oocytes
138 has not been elucidated.
139 In this study, we generated oocyte specific *Zip6* and *Zip10* conditional
140 knockout mice and examined the function of ZIP10 in the oocytes and the role of
141 zinc signaling during fertilization and embryonic development. This study
142 provides clues that elucidate its role in fertilization, which is still largely unknown.
143 In addition, this is the first report confirming the function of the zinc transporter in
144 oocytes, which will contribute to future research.
145
146 **Results**
147 **Zinc transporters, ZIP6, and ZIP10, are expressed in mouse oocytes**
148 **through follicular development**
149 First, using *in situ* hybridization and immunofluorescent staining, we
150 examined the expression of ZIP10 during follicular development. As shown in Fig.
151 1, *Zip10* mRNA was expressed from the primordial oocyte. It continued to be
152 expressed in oocytes of primary, secondary, and antral follicles. ZIP10 protein
153 was also expressed in the plasma membrane of primordial oocytes (Fig.1; Arrow).
154 We also confirmed the expression of ZIP10 protein at the plasma membrane of
155 oocytes of primary, secondary, and antral follicles. Although ZIP6 was also
156 expressed in oocytes throughout folliculogenesis (Fig.1; Arrow), it displayed
157 nuclear localization in oocytes and granulosa cells of primary, secondary, and
158 antral follicles.
159
160 **Phenotype of oocyte-specific *Zip6*$^{d/d}$ and *Zip10*$^{d/d}$ female mice.**
161 To elucidate the roles of *Zip6* and *Zip10* in the mouse oocytes, oocyte-
162 specific *Zip6* (*Zip6*$^{d/d}$) and *Zip10* (*Zip10*$^{d/d}$) knockout mice were generated (Fig.
163 S1*A-C*). *Zip6*$^{f/f}$ and *Zip10*$^{f/f}$ mice were used as controls, respectively. We
164 examined the number of ovulated oocytes or defects in oocyte maturation. After

165 superovulation and ovulation, the number of ovulated oocytes collected from the
166 oviduct in *Zip10*$^{d/d}$ mice was 22.1 ± 2.5 oocytes/mouse (Fig. 2*A*), which was
167 equivalent to that in *Zip10*$^{f/f}$ mice (18.7 ± 2.9 oocytes/mouse, $p > 0.05$). The
168 numbers of ovulated oocytes in *Zip6*$^{d/d}$ and *Zip6*$^{f/f}$ mice were also equivalent (28.7
169 ± 3.6 and 32.8 ± 3.3 oocytes/mice, respectively, $p > 0.05$) (Fig. S2*A*). As for
170 oocyte maturation, the rate of oocytes with a first polar body at 10h, 12h, and 14h
171 in the *Zip10*$^{d/d}$ group was not different than that of *Zip10*$^{f/f}$ group (*Zip10*$^{d/d}$: 58.7%,
172 61.9%, and 79.4%, *Zip10*$^{f/f}$: 50.8%, 54.1% and 70.5%, respectively, $p > 0.05$, Fig.
173 2*B*). In addition, *Zip10*$^{d/d}$ oocytes display intact metaphase spindles just as in the
174 *Zip10*$^{f/f}$ groups (Fig. 2*C*).
175 Next, we examined the levels of labile zinc in germinal vesicle (GV), MII,
176 and two pronuclei (2PN) zygotes by comparing the fluorescence intensity
177 following loading with the dye, FluoZin-3AM (Fig. 2*D*). The FluoZin-3AM
178 fluorescence intensity in GV and MII oocytes of the *Zip10*$^{d/d}$ group was lower than
179 the *Zip10*$^{f/f}$ group ($p < 0.05$). After fertilization, the fluorescence intensity in *Zip10*$^{f/f}$
180 zygotes decreased dramatically, and also decreased for the *Zip10*$^{d/d}$ group,
181 although it remained higher than for *Zip10*$^{f/f}$ oocytes. When compared within
182 group, the fluorescence intensity in *Zip10*$^{f/f}$ between GV and MII oocytes was
183 significantly different (GV vs. MII and MII vs 2PN; $p < 0.05$, respectively), but the
184 stages of *Zip10*$^{d/d}$ oocytes were not different despite clear trends ($p > 0.05$). The
185 levels of zinc fluorescence intensity in the *Zip6*$^{d/d}$ group were not different from
186 the controls *Zip6*$^{f/f}$, which decreased markedly at fertilization (Fig. S2*B*; $p > 0.05$).
187

188 **The zinc sparks of *Zip10*$^{d/d}$ oocytes were suppressed after fertilization or**
189 **artificial activation.**

190 To determine if the absence of ZIP6 and ZIP10 influenced the detection of
191 Zn^{2+} sparks associated with fertilization, we monitored extracellular zinc and
192 intracellular calcium during fertilization of *Zip6*$^{d/d}$ and *Zip10*$^{d/d}$ oocytes (Fig. S3
193 and 3*A*). *Zip10*$^{f/f}$ oocytes displayed the expected calcium oscillations following
194 fertilization, and a zinc spark followed the first calcium rise (Fig. 3*A* upper side,
195 movies 1 and 2). In contrast, *Zip10*$^{d/d}$ oocytes did not release zinc ions
196 immediately after the first calcium spike, despite mounting normal calcium

197 oscillations (Fig. 3*A* lower side, movies 3 and 4). In *Zip6*$^{d/d}$ oocytes, a zinc spark
198 occurred immediately after the first intracellular calcium rise at fertilization, just as
199 in control *Zip6*$^{f/f}$ oocytes (Fig. S3). The extracellular zinc sparks were examined
200 following artificial oocyte activation of mouse oocytes with ionomycin. The zinc
201 sparks occurred immediately after the intracellular calcium rise in *Zip10*$^{f/f}$ oocytes
202 (Fig. 4*B* upper side, movies 5 and 6), however, *Zip10*$^{d/d}$ oocytes did not release
203 zinc ions after the calcium spike (Fig. 3*B* lower side, movies 7 and 8).
204
205 ***Zip10*$^{d/d}$ mouse oocytes can be fertilized but not developed to the blastocyst.**
206 *Zip6*$^{d/d}$ and *Zip10*$^{d/d}$ oocytes then were used for IVF, and we examined the
207 rates of fertilization, polyspermy, and embryo development. Successful
208 fertilization was confirmed at 6 h after IVF by the presence of pronuclei (Fig. 4*A*
209 and *B*). *Zip10*$^{d/d}$ oocytes were fertilized at rates like those observed for control
210 oocytes (Fig. 4*A*). Consistent with this, the zona reaction triggered by fertilization
211 and examined using a ZP2 antibody was similar in *Zip10*$^{d/d}$ and *Zip10*$^{f/f}$ oocytes
212 (Fig. 4*D*). We also examined the localization of ovastacin, whose expression in
213 the cortex and loss post-fertilization was comparable between the two groups (Fig.
214 4*E*). As for the expression of JUNO, it had the same expression than between
215 null and control oocytes and the temporal dynamics of its disappearance from the
216 cortex after fertilization was similar for both *Zip10*$^{f/f}$ and *Zip10*$^{d/d}$ groups (Fig. 4*F*).
217 We next examined the development to the blastocyst stage, and whereas
218 *Zip10*$^{f/f}$ zygotes developed at the expected rates, approximately 75.0%, a smaller
219 fraction of *Zip10*$^{d/d}$ zygotes did and only 32.7% reached this stage ($p < 0.05$) (Fig.
220 4*B*). As shown in Fig. 4*C*, the total cell numbers of blastocysts were also lower
221 for *Zip10*$^{d/d}$ embryos (51.6 ± 2.1 cells) than for those of *Zip10*$^{f/f}$ ones (72.7 ± 2.1
222 cells, $p < 0.05$). *Zip6*$^{d/d}$ oocytes did not display any alterations in the rate of
223 fertilization or development (Fig. S2*C* and *D*; $p > 0.05$).
224
225 **Discussion**
226 The zinc sparks associated with fertilization were first discovered in the
227 mouse. Similar observations followed in other mammalian species and
228 amphibians. However, the underlying mechanism(s) and biological role of zinc

229 sparks are not elucidated. In this study, we have examined the role of the zinc
230 transporters ZIP6 and ZIP10 using conditionally gene deficient mice, and queries
231 their contribution to the zinc sparks of fertilization.

232 First, we confirmed the expression of zinc transporter in mouse oocytes.
233 Our results are consistent with previous studies (21, 38). ZIPs, including ZIP6
234 and ZIP10, are transmembrane proteins (39-42). In primordial follicles, the
235 ooplasmic staining of ZIP10 we anticipate correspond to ooplasmic vesicular
236 sites. ZIP10 expression shifted to the plasma membrane in primary and antral
237 follicle phase. A similar localization shit of ZIP10 to the oocyte surface was
238 reported during oocyte maturation, which is much later than reported here by.
239 Furthermore, in that study, ZIP10 was detected in the nuclear/nucleolar positions
240 of oocytes of all follicular stages (38), which we did not observe. On the other
241 hand, ZIP6 was expressed at the nuclear/nucleolar regions and in granulosa cells.
242 This localization of ZIP6 was consistent with that in a previous study (38).
243 However, our results failed to notice that ZIP6 shifts to the at plasma membrane
244 in antral follicle oocytes (21, 38). The results indicate that ZIP6 may be fulfilling a
245 distinct function within the oocytes compared to ZIP10.

246 To assess the role of these transporters in mice, we generated oocyte-
247 specific *Zip6 or Zip10* knockout mice (Fig. S1; *Zip6*$^{d/d}$ and *Zip10*$^{d/d}$, respectively).
248 Previous reports noted that the disruption of these transporters using specific
249 morpholinos or incubation in function-blocking antibodies induced the change of
250 intracellular labile zinc quota into mice oocytes (21). The amount of free zinc ions
251 in those mouse oocytes was measured using Fluozin-3AM, zinc indicator. The
252 amount of labile zinc ions in *Zip10*$^{d/d}$ oocytes was significantly lower than in the
253 *Zip10*$^{f/f}$ (Fig. *2D*). We failed to observe any effect on zinc levels of in *Zip6*$^{d/d}$
254 oocytes (Fig. *S2B*). The results indicate that ZIP10 is mostly responsible for the
255 uptake of zinc ions in mouse oocytes.

256 Zinc insufficient GV oocytes do not maintain the meiotic arrest at PI. This
257 is suggested to happen by premature activation of the MOS-MAPK pathway in
258 the presence of low zinc (16). In addition, low ooplasmic zinc accelerates meiotic
259 progression that contributes to the extrusion of large polar bodies (18). The early
260 mitotic inhibitor 2 (EMI2), a zinc-binding APC/C proteasome inhibitor, is also an

261 essential component of the cytoplasmic factor (CSF) that initiates entry into MII
262 phase. EMI2 is a zinc binding protein, and when zinc is reduced, the activity of
263 the APC/C proteasome is stimulated, increasing the degradation of CCNB1,
264 reduced MPF activity leading to early release of meiosis arrest (8, 18, 43-45).
265 Previous studies reported that targeted disruption of *Zip10* using morpholino
266 injections and function-inhibiting antibodies during meiotic maturation perturbed
267 meiosis progression and resulted in cell cycle arrest at the telophase I-like state
268 (21). Based on these findings we hypothesized that the reduced state of free zinc
269 ions in *Zip10*$^{d/d}$ mouse oocytes may resemble the state of zinc-deficient oocytes.
270 We investigated the maturation progression and spindle organization in oocyte
271 matured in vitro from the GV to MII stage. We failed to observe any differences
272 (Fig. *2A, B* and *C*). We also did not observed abnormalities in oocytes from *Zip6*$^{f/f}$
273 mice (Fig. *S2A*; $P > 0.05$). We speculate that the disparate outcomes observed
274 in previous studies may be attributed to the presence of trace amounts of zinc
275 ions in media or in the oocytes.

276 Surprisingly, the amount of zinc ions in *Zip10*$^{d/d}$ 2PN zygote was higher
277 than in *Zip10*$^{f/f}$ and despite some differences in fluorescence intensity between
278 *Zip10*$^{d/d}$ GV, MII and 2PN zygote, the labile zinc concentrations were not
279 significantly different between these groups (Fig. *2D*). Therefore, we monitored
280 zinc sparks and calcium oscillations in the *Zip10*-KO oocytes. Several studies
281 reported the important of IP_3Rs in mammalian oocytes (46, 47), which is essential
282 for egg activation because its inhibition precludes Ca^{2+} oscillations (48-50). It has
283 been reported that a putative Zinc-finger motif in a helical linker (LNK) domain
284 near the C-terminus of *IP*$_3$*R1* plays a role in *IP*$_3$*R1* function (51, 52), Recently,
285 Akizawa et al., reported that both deficient and excessive zinc ions compromise
286 *IP*$_3$*R1* sensitivity, diminishing and terminating calcium oscillations (53). Our
287 results showed that a single zinc spark occurs immediately after first calcium rise
288 of oscillations in *Zip10*$^{f/f}$ oocytes, as reported by Kim et al (19) (Fig. *3A*), and
289 similar results are obtained in *Zip6*$^{d/d}$ and *Zip6*$^{f/f}$ mouse oocytes (Fig. *S3*).
290 However, in *Zip10*$^{d/d}$ oocytes, despite the presence calcium elevations, zinc
291 sparks failed to occur. Similarly, *Zip10*$^{d/d}$ oocytes activated with ionomycin
292 (artificial oocyte activation) did not show a zinc spark (Fig. *3B*). In this study,

293 calcium oscillations occurred in oocytes with low zinc state. In addition, there was
294 no difference in the amplitude frequency of calcium ions in oocytes of both groups
295 within the observation time. Akizawa et al., produced zinc deficiency state with
296 TPEN, a strong chelator of intracellular labile zinc ions (53). On the other hand,
297 we did not completely remove intracellular labile zinc ions from mouse oocytes.
298 We speculate that zinc ions existed in *Zip10*$^{d/d}$ mouse oocytes induce Ca^{2+}
299 release without compromising *IP*$_3$*R1* sensitivity. However, this study
300 demonstrated that the accumulation of intracellular zinc ions mediated by ZIP10
301 is essential for inducing zinc sparks in mouse oocytes.

302 The total cellular zinc ions content required for meiosis in the oocyte
303 substantially increases (a 50% increase) from the prophase I arrest to the arrest
304 at metaphase of meiosis II (17, 18). The zinc is stored in undefined cortical
305 granules, and an average of 10^6 zinc atoms are released from these vesicles at
306 the time of fertilization (exocytosis) (19-23, 25). There are several possibilities
307 that might explain why *Zip10* conditional KO mice have low zinc sparks. The most
308 logical is that these oocytes experience reduced zinc loading of cortical of zinc
309 vesicles, leading to the absence of sparks. Our results suggest that in oocytes,
310 zinc sparks and exocytosis require adequate concentrations of zinc ions in the
311 cortical secretory vesicles, which is not accomplished when ZIP10 is not present.

312 Zinc sparks have been reported to contribute to the rapid and permanent
313 block mechanisms to prevent polyspermy. The former is achieved by zinc in the
314 extracellular milieu decelerating the forward motility of sperm (29). Secondly, the
315 release of labile pools of zinc at the same time that the zinc metalloendopeptidase
316 ovastacin is released with the cortical granules (29, 54, 55), cause ZP2 protein
317 cleavage inducing a complete, although belated block to polyspermy (24, 28, 29).
318 However, the physiological significance of the zinc sparks' contributions to
319 polyspermy have not been thoroughly tested, and *Zip10*$^{d/d}$ mice, which are almost
320 devoid of them, offer a great model. Our results showing normal rates of
321 monospermic fertilization in *Zip10*$^{d/d}$ *oocyte* suggest that contributions of Zinc to
322 polyspermy control is negligible (Fig. *4A*). Our results also show that the
323 ovastacin undergoes normal release in *Zip10*$^{f/f}$ oocytes after fertilization (Fig. *4E*
324 and 4*D*), confirming previous studies of a minor role of the ZP2 to polyspermy.

325 We observed the disappearance of JUNO after fertilization (56) *Zip10*$^{d/d}$,
326 suggesting that gamete fusion took place (Fig. *4F*). Together, these results
327 support the view that zinc spark is not directly involved in the polyspermy rejection
328 mechanism.

329 Interestingly, there were no differences in the rates of fertilization
330 (pronucleus formation), but development to the blastocyst stage was significantly
331 reduced in *Zip10*-null embryos (Fig. *4B*). These embryos seem to gradually arrest
332 after the 2-cell stage (data not shown) and lose viability. It is well known that zinc
333 levels play a role in embryonic development. Zinc insufficiency caused altered
334 chromatin structure in the nuclei of blastomeres that displayed decreased global
335 transcription, causing arrest in embryonic development (57). The abnormal zinc
336 homeostasis, particularly during the one-cell stage, inhibits the activation of the
337 embryonic genome that occurs around the two-cell stage in mice due to reduce
338 the translational capacity through the inhibition of ribosomal RNA synthesis by
339 RNA polymerase I (10, 58). Our results also show that *Zip10*$^{d/d}$ blastocysts had
340 significantly lower cell numbers compared to the blastocysts from *Zip10*$^{f/f}$ mice
341 (Fig. *4C*). Our results suggest that Zip10$^{d/d}$ mice oocytes can be fertilizable, but
342 their developmental potential is decreased. The lack of ZIP10-mediated zinc
343 influx during the folliculogenesis of *Zip10*$^{d/d}$ may compromise gene expression
344 during these early stages of oocyte development. *Zip10*$^{d/d}$ mouse oocytes thus
345 may have compromised developmental potential from the outset. Future studies
346 should assess the transcriptomic profile of *Zip10*$^{d/d}$ mouse oocytes.

347 In conclusion, we elucidated that ZIP10 is required for zinc ion uptake into
348 oocytes and the intracellular zinc ions regulated by ZIP10 was important for zinc
349 sparks and progression of embryonic development. Currently, the many infertility
350 patients exist in the world (the survey of WHO). It is reported that approximately
351 half of the adult females are deficient in zinc in their serum (59, 60). Zinc has
352 been reported to play essential roles in many physiological functions including
353 reproductive functions. The findings will help elucidate the role of zinc signaling
354 in the fields of fertilization/embryogenesis. Furthermore, the development of zinc-
355 focused assisted reproductive technologies and fertilization/embryogenesis
356 media could contribute to improve the developmental potential of oocytes and

357 embryos in other mammalian species.
358
359 **Materials and Methods**
360 All chemicals and reagents were purchased from Sigma-Aldrich (St. Louis, MO,
361 USA) unless otherwise stated.
362
363 **Animals**
364 Animals were housed in the barrier facility at Azabu University. The
365 deletion of the ZIP10 gene in the whole body is known to result in embryonic
366 lethality (37). The conditional knockout mice were generated by Cre-loxP system.
367 The following mouse strains were used: *Zip10*$^{flox/flox}$ (*Zip10*$^{f/f}$) mouse <B6;129-
368 Slc39a10 <tm1.1Tfk>> (RBRC06221) (35, 61, 62) was provided by the RIKEN
369 BRC through the National BioResource Project of the MEXT/AMED, Japan.
370 *Zip6*$^{flox/flox}$ (*Zip6*$^{f/f}$) mouse <B6;129-Slc39a6> was generated by AdAMS. *Gdf9*$^{Cre/+}$
371 mice <Stock Tg (GDF9-iCre) 5092Coo/J, Stock No: 011062> were delivered from
372 Jackson Laboratory (63). Crlj: C57BL/6J female mice (6-8 weeks old) and Crlj:
373 C57BL/6J male mice (8-12 weeks old) were purchased from Charles River
374 Laboratories Japan (Yokohama, Japan). The mice were housed under controlled
375 lighting conditions (daily light period, 0600-1800 h). The study was approved by
376 the Animal Experimentation Committees of Azabu University and were performed
377 in accordance with the committees' guidelines (200318-13 and 230309-1).
378 Oocyte-specific gene knockout (*Zip10*$^{f/f}$, *Gdf9*$^{Cre/+}$; *Zip10*$^{d/d}$) mice were generated
379 by crossing *Gdf9*$^{Cre/+}$ male mice with *Zip10*$^{f/f}$ female mice (Fig. S1*A*-*E*). Similarly,
380 *Zip6*$^{d/d}$ mice were generated (Fig. S1*A*-*E*).
381
382 **In situ hybridization (ISH)**
383 ISH was performed as previously described with some modifications (64).
384 Briefly, fixed ovaries were paraffin-embedded and paraffin sections (6 μm) were
385 mounted on MAS-coated slides (Matsunami Glass Industries, Osaka, Japan)
386 under RNase-free conditions. Sense or antisense digoxigenin (DIG)-labeled RNA
387 probes for *Slc39a10* (*Zip10*) were purchased from Genostaff. The sections were
388 deparaffinized, rehydrated, and post-fixed in 10% neutral buffered formalin (NBF)

389 for 30 min at 37°C, followed by the treatment with 0.2% hydrogen chloride and 5
390 μg/ml proteinase K (FUJIFILM Wako Pure Chemical, Osaka, Japan) for 10 min
391 at 37°C, respectively. Hybridization was performed with DIG-labeled probes (250
392 ng/ml) in a humidified chamber at 60°C overnight. The slides were washed after
393 hybridization, then treated with blocking reagent (Genostaff) for 15 min and
394 alkaline phosphatase-conjugated anti-DIG antibody (1:2,000; Roche Diagnostics,
395 Basel, Switzerland) for 1 h at room temperature. The signals were detected by 4-
396 nitro-blue tetrazolium/5-bromo-4-chloro-3-indolyl phosphate (NBT/BCIP, Roche
397 Diagnostics) in a humidified container for 12 h at 4°C. The sections were
398 counterstained with Kernechtrot solution (Muto Pure Chemicals, Tokyo, Japan).
399 Signals detected by the sense probe were used as a control for background levels.
400

401 **Immunofluorescent staining (IF) for ovary**

402 IF was performed as previously described with some modifications (64).
403 Fixed ovaries were paraffin-embedded and the sections (6 μm) were
404 deparaffinized, hydrated and conducted for antigen retrieval by autoclaving in 10
405 mM sodium citrate buffer (pH = 6.0) for 5 min. The sections were further incubated
406 on ice for 30 min. After blocking with Bloking One Histo (06349-64, NACALAI
407 TESQUE Inc, Kyoto, Japan) for 1 h, the slides were incubated with primary
408 antibody for Rabbit anti-mouse-Zip10 (1:200; (62)), Rabbit anti-SLC39A6 (1:200,
409 HPA042377, Sigma), Rabbit anti-Foxl2 (1:300; (65, 66)), Rat anti-ZP2 (1:100, sc-
410 32752, Santa Crus Biotechnology, Dallas, Texas, USA) in Can Get Signal
411 immunostain (TOYOBO, Tokyo, Japan) overnight at 4°C. The slides were
412 incubated with Alexa Fluor 488 donkey anti-rabbit IgG (H+L), Alexa Fluor 594
413 donkey anti-rabbit IgG (H+L) or Alexa Fluor 488 donkey anti-rat IgG (H+L)
414 conjugated secondary antibodies (Jackson Immuno Research Laboratories,
415 West Grove, PA, USA) diluted 1:500 in Can Get Signal immunostain (TOYOBO)
416 for 1 h, and mounted with ProLong Glass Antifade Mountant with NucBlue Stain
417 (P36981, Thermo Fisher Scientific, Waltham, MA, USA). Micrographs were
418 captured by BZ-X700 microscopy (Keyence, Osaka, Japan).
419

420 **Oocyte preparation**

421 Germinal vesicle (GV) oocytes were collected in the manner described in
422 our previous study (67) with some modifications. Ovaries were collected from
423 female mice 48 h after intraperitoneally injection with 5 IU equine chorionic
424 gonadotropin (eCG) (PMS; Nippon Zenyaku Kogyo, Fukushima, Japan). They
425 were placed in a 35 mm culture dish containing MEMα (no nucleosides, powder;
426 Gibco/Thermo Fisher Scientific, Tokyo, Japan) medium with 26 mM $NaHCO_3$, 75
427 mg/l penicillin, 50 mg/l streptomycin sulfate, 5% (v/v) heat-treated fetal calf serum
428 (FCS), and 10 ng/ml epidermal growth factor (EGF). Cumulus-oocyte complexes
429 (COCs) were released from the antral follicles by gentle puncturing with a needle.
430 To obtain metaphase II (MII) oocytes, the mice were intraperitoneally
431 injected with 5 IU eCG followed by injection with 5 IU human chorionic
432 gonadotropin (hCG) (Gonatropin; ASKA Pharmaceutical, Tokyo, Japan) at 48 h
433 later. COCs were collected from the oviductal ampulla 14-16 h after hCG injection.
434 These oocytes were used in the following experiments.
435
436 **Count of ovulated oocytes**
437 COCs-MII were obtained by superovulation treatment. The cumulus cells
438 were removed from the COCs-MII with hyaluronidase (1 mg/ml) and gentle
439 pipetting. All collected oocytes were counted and calculated as the number of
440 ovulations.
441
442 **In vitro maturation (IVM) of GV oocytes**
443 IVM were conducted in the manner described in our previous study (68)
444 with some modifications. Ovaries were placed in a 35 mm culture dish containing
445 MEMα medium with 26 mM $NaHCO_3$, 75 mg/l penicillin, 50 mg/l streptomycin
446 sulfate, 5% (v/v) FCS, and 10 ng/ml EGF. COCs-GV were released from the
447 antral follicles by gentle puncturing with a needle. The COCs-GV were washed 3
448 times and cultured in 500 μl of same medium in 4-well dish at 37°C in an
449 atmosphere of 5% CO_2 in air for 10, 12 and 14 h. After the culture, cumulus cells
450 were removed from the COCs with hyaluronidase (1 mg/ml) and gentle pipetting.
451 The extrusion of 1st polar body was evaluated at each time.
452

453 **IF for oocytes/preimplantation embryos**

454 The α-tubulin and JUNO (PE anti-mouse FR4) were performed with some
455 modification of the methods of Inoue et al (69). The oocytes or embryos were
456 fixed in 4% PFA for 30 min at room temperature, washed in PBS containing 1%
457 polyvinyl alcohol (PBS/PVA). They were permeabilized by treatment of 0.5%
458 Triton X-100 for 15 min and washed 2 times in 1% BSA/PBS/PVA followed by
459 blocked for 20 min in same medium. They were incubated for overnight at 4° with
460 primary antibodies to rabbit anti-α-tubulin (1:200; 11H10, cell Signaling
461 Technology) or rat anti-mouse FR4 (JUNO; 1:250; 12A5 BioLegend), wash 3
462 times in 1% BSA/PBS/PVA. Primary antibodies were detected using Alexa Fluor
463 488 donkey anti-rabbit IgG (H+L) (1:250) or Alexa Fluor 488 donkey anti-rat IgG
464 (H+L) (1:250) for 1 h at room temperature. After staining, all samples mounted in
465 VECTASHIELD Mounting Medium with DAPI (H-1200; Vector Laboratories,
466 California, USA), imaged using BZ-X700 microscopy (Keyence, Osaka, Japan).

467 The ovastacin staining was performed with some modifications of the
468 methods of Burkart et al (54). oocytes or embryos were fixed in 4% PFA for
469 overnight at 4 ^{o}C, washed in PBS containing 0.3% polyvinylpyrrolidone (PVP),
470 and then blocked in 0.3% BSA/0.1 M glycine (three times for 10 min) followed by
471 permeabilization in 0.2% Triton X-100 for 15 min (70). Samples were then
472 incubated for overnight at 4°C with Rabbit polyclonal anti-ovastacin (54), 1:200,
473 gifted antibody), washed with 0.3% PVP/0.1% Tween (three times for 10 min),
474 and incubated for 1 h at room temperature with Alexa Fluor 488 anti-rabbit
475 secondary antibody (1:500) followed by staining and mounting with
476 VECTASHIELD Mounting Medium with DAPI. Samples were imaged using TCS
477 SP5 II confocal microscope (Leica Microsystems, Wetzlar, Germany).

478

479 **In vitro fertilization (IVF)**

480 IVF and sperm collection were conducted with some modification of the
481 method described in our previous study (71). In brief, ovulated COCs-MII were
482 preincubated for 1 h in 80 μl human tubal fluid (HTF) droplets supplemented with
483 1.25 mM reduced glutathione (GSH). Frozen-thawed sperm suspensions were

484 suspended in 200 μl preincubation medium (HTF containing 0.4 mM methyl-β-
485 cyclodextrin) and 0.1 mg/ml PVA, but without bovine serum albumin, and were
486 incubated at 37 °C under 5% CO_2 in humidified air for 1 h. At the time of
487 insemination, preincubated spermatozoa were transferred into the droplets with
488 oocytes at final concentrations of 2.0×10^6 sperm/ml. After 6 h, oocytes were
489 separated from spermatozoa and cumulus cells using a fine glass pipette and
490 transferred into 50 μl KSOMaa medium. They were cultured at 37 °C under 5%
491 CO_2 in humidified air for approximately 24-96 h. After IVF at 96 h, the blastocysts
492 were fixed in 4% PFA for 30 min at room temperature. Following three times
493 washed in PBS/PVA for 30 min each. Nuclear DNA was stained and mounted in
494 VECTASHIELD Mounting Medium with DAPI. Cell numbers were determined by
495 visually inspecting nuclei stained with DAPI using an inverted fluorescence
496 microscope.
497

498 **Zinc measurements**

499 FluoZin-3AM staining was conducted using the method described in our
500 previous study (72). The obtained GV oocytes, cumulus cells were removed from
501 the COCs with gentle pipetting. The obtained MII oocytes, cumulus cells were
502 removed from the COCs with hyaluronidase (1 mg/ml) and gentle pipetting.
503 Oocytes with a polar body were defined as MII. After IVF for 6h, two pronucleus
504 stage embryos (2PN) were collected. GV, MII and 2PN were loaded in 50 μl
505 medium that was suitable for each stage containing the amyl ester of the
506 membrane permeant zinc-specific fluorophore, FluoZin-3AM (2 μM; F24195,
507 Thermo Fisher Scientific, excitation 494 nm/emission 516 nm) for 1 h in
508 humidified CO_2 [5% (v/v) in air] at 37 °C followed by washing three times in
509 medium and then observation with TCS SP5 II confocal microscope. The pixel
510 intensity per unit area after background subtraction was determined in GV, MII
511 and 2PN within the circle (white circle) and ImageJ image processing software.
512

513 **Measurement of Ca^{2+} and Zinc spark during fertilization**

514 *Zip10$^{f/f}$* and *Zip10$^{d/d}$* female mice (7-12weeks) were treated for
515 superovulation with eCG and hCG as same procedure. COCs were collected at

516 14-16 h after hCG injection and removed cumulus cells with hyaluronidase. The
517 zona pellucida (ZP) was removed by brief treatment in acidic Tyrode's solution.
518 The ZP-free MII were cultured in HTF containing Calbryte™ 590 AM (10 μM,
519 excitation 581 nm/emission 593 nm; AAT Bioquest, CA, USA) for 10-20 min in
520 humidified CO_2 [5% (v/v) in air] at 37 °C. In case of IVF, ZP-free MII were allowed
521 to settle in 5 μl calcium-free HTF medium drop on dish to attach oocytes. After
522 attached, HTF medium that contained BSA and membrane impermeant zinc-
523 specific fluorophore, FluoZin-3 (20 μM; F24194, Thermo Fisher Scientific,
524 excitation 494 nm/emission 516 nm) was slowly added to a final volume of 45 μl,
525 taking care not to disturb oocytes, to start imaging. In case ionomycin treatment,
526 after calcium labeling, ZP-free MII were allowed to settle in 45 μl calcium-free
527 HEPES-CZB medium drop on dish, to start imaging. Imaging was performed on
528 confocal microscope using 488 nm (Zn^{2+}) and 555 nm (Ca^{2+}) excitation (Nikon
529 solutions, Tokyo, Japan) for max 50 min every 4 seconds. Capacitated frozen-
530 thawed sperm or 5 μM ionomycin were added to ZP-free MII at 2 min after
531 imaging start. Imaging analysis was performed by defining regions of interest
532 (ROIs) and measuring fluorescence intensity over time using NIS-Elements
533 (Nikon). The intracellular ROIs were drawn as the entire interior area of the cell.
534 The extracellular ROIs were defined as a ring around the perimeter of cell. The
535 ring thickness was conserved for all data analyses. The same methos was used
536 for the *Zip6*$^{f/f}$ and *Zip6*$^{d/d}$ *mice*.
537
538 **Western blotting**
539 Western blotting was carried out as described (73) with some
540 modifications. Thirty MII oocytes or 2PN embryos were lysed in Laemmli sample
541 buffer (Bio-Rad Laboratories, Tokyo, Japan) with 5% 2-mercaptoethanol.
542 Samples were separated on 8% Bis-Tris gels by SDS-PAGE and transferred to
543 PVDF membranes (Bio-Rad). The PVDF membranes were blocked in 10% skim
544 milk (FUJIFILM Wako) in Tris-buffered saline (TBS) with 0.1% Tween-20
545 (Yoneyama yakuhin kogyo, Osaka, Japan) and probed with primary antibody to
546 rat anti-ZP2 (1:1,000) or monoclonal mouse anti-β-actin (1:5,000; A5316, Sigma-
547 Aldrich) for overnight at 4°C. The membranes were incubated with secondary

548 antibody; HRP-conjugated anti-rat IgG (1:5000; Cell Signaling Technology) or
549 HRP-conjugated anti-mouse IgG (1:5,000; Cell Signaling Technology) for 1 h at
550 room temperature. After washing of the membranes, immunoreactive proteins
551 were visualized using ECL^{TM} Western Blotting Analysis System (Cytiva Global
552 Life Sciences Technologies, Tokyo, Japan), according to the manufacture's
553 recommendation. The membranes were exposed by ImageQuant LAS 4000.
554
555 **Statistical analysis**
556 Values from three or more times were used for evaluation of statistical
557 significance. Statistical analysis was performed using Statcel 3 software (OMS
558 Ltd., Saitama, Japan). The fertility, the total numbers of oocytes collected from
559 each mouse, the percentage of first polar extrusions, the fluorescence intensity
560 of Fluozin-3 AM and the cell count of blastocysts were evaluated statistically by
561 Student's t-test analysis. The rate of fertilization and embryo development was
562 analyzed using chi square tests. Values are shown as means ± S.E.M, and
563 significant differences were considered at p values < 0.05.
564
565
566 **Acknowledgments and funding sources**
567 We thank the members of the Laboratory of Animal Reproduction, School of
568 Veterinary Medicine, Azabu University for technical help. *Zip10*$^{flox/flox}$ (*Zip10*$^{f/f}$)
569 mouse <B6;129-Slc39a10 <tm1.1Tfk>> (RBRC06221) was provided by the
570 RIKEN BRC through the National BioResource Project of the MEXT/AMED,
571 Japan. We also thank Dr. Austin J. Cooney (The University of Texas at Austin,
572 Austin, United States) for providing GDF9-iCre mice. This research was
573 supported by Grants-in-Aid for Scientific Research from the Japan Society for the
574 Promotion of Science (JSPS) (KAKENHI, 21H02384 and 20H05373 to J.I.,
575 22H04268 and 24H02601 to A.K.), JSPS KAKENHI Grant Number JP 15H04584
576 (AdAMS) to JI, the Sasakawa Scientific Research Grant from The Japan Science
577 Society (2019-4044) to A.K. and Mishima Kaiun Memorial Foundation (A-135) to
578 A.K. This work was supported by JSPS KAKENHI Grant Number JP 22H04922
579 (AdAMS). This study was also supported by Center for Diversity, Equity &

Inclusion, Azabu University (A.K). This research was partially supported by the Center for Human and Animal Symbiosis Science, Azabu University and a research project grant awarded by the Azabu University Research Services Division to J.I.

References

1. S. Yoon, R. A. Fissore, Release of phospholipase C zeta and [Ca2+]i oscillation-inducing activity during mammalian fertilization. *Reproduction.* **134**, 695-704 (2007).

2. C. M. Saunders *et al.,* PLC zeta: A sperm-specific trigger of ca(2+) oscillations in eggs and embryo development. *Development.* **129**, 3533-3544 (2002).

3. Z. Xu, G. S. Kopf, R. M. Schultz, Involvement of inositol 1,4,5-trisphosphate-mediated Ca2+ release in early and late events of mouse egg activation. *Development.* **120**, 1851-1859 (1994).

4. K. T. Jones, Mammalian egg activation: From Ca2+ spiking to cell cycle progression. *Reproduction.* **130**, 813-823 (2005).

5. T. Ducibella, R. M. Schultz, J. Ozil, Role of calcium signals in early development. *Semin. Cell. Dev. Biol.* **17**, 324-332 (2006).

6. J. Ito, J. Parrington, R. A. Fissore, PLCzeta and its role as a trigger of development in vertebrates. *Mol. Reprod. Dev.* **78**, 846-853 (2011).

7. H. Sugita *et al.,* Molecular mechanism of oocyte activation in mammals: Past, present, and future directions. *Biomolecules.* **14**, 359 (2024).

8. T. Suzuki *et al.,* Full-term mouse development by abolishing Zn2+-dependent metaphase II arrest without Ca2+ release. *Development.* **137**, 2659-2669 (2010).

9. D. Allouche-Fitoussi, H. Breitbart, The role of zinc in male fertility. *Int. J. Mol. Sci.* **21**, 7796 (2020).

10. A. Kageyama, J. Terakawa, J. Ito, N. Kashiwazaki, Roles of zinc signaling in mammalian reproduction. Metallomics Research. **2**, 2022.

611 11. S. Lubna, R. Ahmad, Clinical and biochemical understanding of zinc
612 interaction during liver diseases: A paradigm shift. *J. Trace. Elem. Med. Biol.*
613 **77**, 127130 (2023).

614 12. A. M. Pascua *et al.,* Reproductive hormones influence zinc homeostasis in
615 the bovine cumulus-oocyte complex: Impact on intracellular zinc concentration
616 and transporters gene expression. *Theriogenology.* **146**, 48-57 (2020).

617 13. A. E. Favier, The role of zinc in reproduction. hormonal mechanisms. *Biol.*
618 *Trace. Elem. Res.* **32**, 363-382 (1992).

619 14. R. S. Bedwal, A. Bahuguna, Zinc, copper and selenium in reproduction.
620 *Experientia.* **50**, 626-640 (1994).

621 15. X. Tian, F. J. Diaz, Zinc depletion causes multiple defects in ovarian
622 function during the periovulatory period in mice. *Endocrinology.* **153**, 873-886
623 (2012).

624 16. B. Y. Kong *et al.,* Zinc maintains prophase I arrest in mouse oocytes
625 through regulation of the MOS-MAPK pathway. *Biol. Reprod.* **87**, 1-12 (2012).

626 17. A. M. Kim, S. Vogt, T. V. O'Halloran, T. K. Woodruff, Zinc availability
627 regulates exit from meiosis in maturing mammalian oocytes. *Nat. Chem. Biol.* **6**,
628 674-681 (2010).

629 18. M. L. Bernhardt, A. M. Kim, T. V. O'Halloran, T. K. Woodruff, Zinc
630 requirement during meiosis I-meiosis II transition in mouse oocytes is
631 independent of the MOS-MAPK pathway. *Biol. Reprod.* **84**, 526-536 (2011).

632 19. A. M. Kim *et al.,* Zinc sparks are triggered by fertilization and facilitate cell
633 cycle resumption in mammalian eggs. *ACS. Chem. Biol.* **6**, 716-723 (2011).

634 20. E. L. Que *et al.,* Quantitative mapping of zinc fluxes in the mammalian egg
635 reveals the origin of fertilization-induced zinc sparks. *Nat. Chem.* **7**, 130-139
636 (2015).

637 21. B. Y. Kong *et al.,* Maternally-derived zinc transporters ZIP6 and ZIP10 drive
638 the mammalian oocyte-to-egg transition. *Mol. Hum. Reprod.* **20**, 1077-1089
639 (2014).

640 22. E. L. Que *et al.,* Bovine eggs release zinc in response to parthenogenetic
641 and sperm-induced egg activation. *Theriogenology.* **127**, 41-48 (2019).

642 23. Y. Jo *et al.,* Spire localization via zinc finger-containing domain is crucial for
643 the asymmetric division of mouse oocyte. *Faseb. J.* **33**, 4432-4447 (2019).

24. E. L. Que *et al.,* Zinc sparks induce physiochemical changes in the egg zona pellucida that prevent polyspermy*. Integr. Biol. (Camb).* **9**, 135-144 (2017).

25. H. C. Lee *et al.,* Zinc exocytosis is sensitive to myosin light chain kinase inhibition in mouse and human eggs*. Mol. Hum. Reprod.* **26**, 228-239 (2020).

26. F. E. Duncan *et al.,* The zinc spark is an inorganic signature of human egg activation*. Sci. Rep.* **6**, 24737 (2016).

27. J. F. Seeler *et al.,* Metal ion fluxes controlling amphibian fertilization*. Nat. Chem.* **13**, 683-691 (2021).

28. S. Aonuma, M. Okabe, M. Kawaguchi, Y. Kishi, Zinc effects on mouse spermatozoa and in-vitro fertilization*. J. Reprod. Fertil.* **63**, 463-466 (1981).

29. K. Tokuhiro, J. Dean, Glycan-independent gamete recognition triggers egg zinc sparks and ZP2 cleavage to prevent polyspermy*. Dev. Cell.* **46**, 627-640.e5 (2018).

30. T. Fukada, T. Kambe, Molecular and genetic features of zinc transporters in physiology and pathogenesis*. Metallomics.* **3**, 662-674 (2011).

31. T. Takagishi, T. Hara, T. Fukada, Recent advances in the role of SLC39A/ZIP zinc transporters in vivo*. Int. J. Mol. Sci.* **18**, 2708 (2017).

32. T. Kambe, T. Tsuji, A. Hashimoto, N. Itsumura, The physiological, biochemical, and molecular roles of zinc transporters in zinc homeostasis and metabolism*. Physiol. Rev.* **95**, 749-784 (2015).

33. K. M. Taylor *et al.,* Zinc transporter ZIP10 forms a heteromer with ZIP6 which regulates embryonic development and cell migration*. Biochem. J.* **473**, 2531-2544 (2016).

34. D. Pal, U. Sharma, S. K. Singh, R. Prasad, Association between ZIP10 gene expression and tumor aggressiveness in renal cell carcinoma*. Gene.* **552**, 195-198 (2014).

35. B. Bin *et al.,* Requirement of zinc transporter ZIP10 for epidermal development: Implication of the ZIP10-p63 axis in epithelial homeostasis*. Proc. Natl. Acad. Sci. U. S. A.* **114**, 12243-12248 (2017).

36. K. Nakajima *et al.,* Possible involvement of zinc transporter ZIP10 in atopic dermatitis*. J. Dermatol.* **47**, e51-e53 (2020).

37. X. He *et al.,* The zinc transporter SLC39A10 plays an essential role in embryonic hematopoiesis*. Adv. Sci. (Weinh).* **10**, e2205345 (2023).

677 38. Y. Chen *et al.,* Zinc dynamics regulate early ovarian follicle development*. J.*
678 *Biol. Chem.* **299**, 102731 (2023).

679 39. D. J. Eide, The SLC39 family of metal ion transporters*. Pflugers. Arch.* **447**,
680 796-800 (2004).

681 40. T. Kambe, Y. Yamaguchi-Iwai, R. Sasaki, M. Nagao, Overview of
682 mammalian zinc transporters*. Cell. Mol. Life. Sci.* **61**, 49-68 (2004).

683 41. M. Lu, D. Fu, Structure of the zinc transporter YiiP*. Science.* **317**, 1746-
684 1748 (2007).

685 42. G. Schmitt-Ulms *et al.,* Evolutionary descent of prion genes from the ZIP
686 family of metal ion transporters*. PLoS One.* **4**, e7208 (2009).

687 43. M. L. Bernhardt *et al.,* A zinc-dependent mechanism regulates meiotic
688 progression in mammalian oocytes*. Biol. Reprod.* **86**, 114 (2012).

689 44. S. Shoji *et al.,* The zinc-binding region (ZBR) fragment of Emi2 can inhibit
690 APC/C by targeting its association with the coactivator Cdc20 and UBE2C-
691 mediated ubiquitylation*. FEBS. Open. Bio.* **4**, 689-703 (2014).

692 45. M. Ohe *et al.,* Emi2 inhibition of the anaphase-promoting
693 complex/cyclosome absolutely requires Emi2 binding via the C-terminal RL tail*.*
694 *Mol. Biol. Cell.* **21**, 905-913 (2010).

695 46. R. A. Fissore *et al.,* Differential distribution of inositol trisphosphate receptor
696 isoforms in mouse oocytes*. Biol. Reprod.* **60**, 49-57 (1999).

697 47. J. Parrington *et al.,* Expression of inositol 1,4,5-trisphosphate receptors in
698 mouse oocytes and early embryos: The type I isoform is upregulated in oocytes
699 and downregulated after fertilization*. Dev. Biol.* **203**, 451-461 (1998).

700 48. S. Miyazaki, M. Ito, Calcium signals for egg activation in mammals*. J.*
701 *Pharmacol. Sci.* **100**, 545-552 (2006).

702 49. S. Miyazaki *et al.,* Block of Ca2+ wave and Ca2+ oscillation by antibody to
703 the inositol 1,4,5-trisphosphate receptor in fertilized hamster eggs*. Science.*
704 **257**, 251-255 (1992).

705 50. Z. Xu, C. J. Williams, G. S. Kopf, R. M. Schultz, Maturation-associated
706 increase in IP3 receptor type 1: Role in conferring increased IP3 sensitivity and
707 Ca2+ oscillatory behavior in mouse eggs*. Dev. Biol.* **254**, 163-171 (2003).

708 51. G. Fan *et al.,* Gating machinery of InsP3R channels revealed by electron
709 cryomicroscopy*. Nature.* **527**, 336-341 (2015).

710 52. N. Paknejad, R. K. Hite, Structural basis for the regulation of inositol
711 trisphosphate receptors by ca(2+) and IP(3). *Nat. Struct. Mol. Biol.* **25**, 660-668
712 (2018).

713 53. H. Akizawa, E. Lopes, R. A. Fissore, Zn(2+) is essential for ca(2+)
714 oscillations in mouse eggs. *bioRxiv.* (2023).

715 54. A. D. Burkart *et al.,* Ovastacin, a cortical granule protease, cleaves ZP2 in
716 the zona pellucida to prevent polyspermy. *J. Cell. Biol.* **197**, 37-44 (2012).

717 55. C. Schmitz *et al.,* The E-modulus of the oocyte is a non-destructive measure
718 of zona pellucida hardening. *Reproduction.* **162**, 259-266 (2021).

719 56. E. Bianchi, B. Doe, D. Goulding, G. J. Wright, Juno is the egg izumo
720 receptor and is essential for mammalian fertilization. *Nature.* **508**, 483-487
721 (2014).

722 57. B. Y. Kong *et al.,* The inorganic anatomy of the mammalian preimplantation
723 embryo and the requirement of zinc during the first mitotic divisions. *Dev. Dyn.*
724 **244**, 935-947 (2015).

725 58. G. F. Chanfreau, Zinc'ing down RNA polymerase I. *Transcription.* **4**, 217-
726 220 (2013).

727 59. A. S. Prasad, Zinc deficiency in women, infants and children. *J. Am. Coll.*
728 *Nutr.* **15**, 113-120 (1996).

729 60. H. Yokokawa *et al.,* Serum zinc concentrations and characteristics of zinc
730 deficiency/marginal deficiency among japanese subjects. *J. Gen. Fam. Med.* 21,
731 248-255 (2020).

732 61. S. Hojyo *et al.,* Zinc transporter SLC39A10/ZIP10 controls humoral
733 immunity by modulating B-cell receptor signal strength. *Proc. Natl. Acad. Sci. U.*
734 *S. A.* **111**, 11786-11791 (2014).

735 62. T. Miyai *et al.,* Zinc transporter SLC39A10/ZIP10 facilitates antiapoptotic
736 signaling during early B-cell development. *Proc. Natl. Acad. Sci. U. S. A.* **111**,
737 11780-11785 (2014).

738 63. Z. Lan, X. Xu, A. J. Cooney, Differential oocyte-specific expression of cre
739 recombinase activity in GDF-9-iCre, Zp3cre, and Msx2Cre transgenic mice.
740 *Biol. Reprod.* **71**, 1469-1474 (2004).

741 64. T. Namiki *et al.,* Uterine epithelial Gp130 orchestrates hormone response
742 and epithelial remodeling for successful embryo attachment in mice. *Sci. Rep.*
743 **13**, 854-y (2023).

744 65. J. Cocquet *et al.,* Evolution and expression of FOXL2*. J. Med. Genet.* **39**,
745 916-921 (2002).

746 66. J. C. Polanco *et al.,* Sox10 gain-of-function causes XX sex reversal in mice:
747 Implications for human 22q-linked disorders of sex development*. Hum. Mol.*
748 *Genet.* **19**, 506-516 (2010).

749 67. J. Ito *et al.,* Inositol 1,4,5-trisphosphate receptor 1, a widespread Ca2+
750 channel, is a novel substrate of polo-like kinase 1 in eggs*. Dev. Biol.* **320**, 402-
751 413 (2008).

752 68. M. Kamoshita, K. Fujiwara, J. Ito, N. Kashiwazaki, Highly successful
753 production of viable mice derived from vitrified germinal vesicle oocytes*. PLoS*
754 *One.* **16**, e0248050 (2021).

755 69. A. Inoue *et al.,* Maternal H3K27me3 controls DNA methylation-independent
756 imprinting*. Nature.* **547**, 419-424 (2017).

757 70. B. Baibakov *et al.,* Sperm binding to the zona pellucida is not sufficient to
758 induce acrosome exocytosis*. Development.* **134**, 933-943 (2007).

759 71. A. Kageyama *et al.,* A combined treatment with progesterone, anti-inhibin
760 serum, and equine chorionic gonadotropin improves number of ovulated
761 oocytes in young C57BL/6J mice*. J. Reprod. Dev.* **69**, 223-226 (2023).

762 72. A. Kageyama *et al.,* Dynamic changes of intracellular zinc ion level during
763 maturation, fertilization, activation, and development in mouse oocytes*. Anim.*
764 *Sci. J.* **93**, e13759 (2022).

765 73. J. Ito *et al.,* Phosphorylation of inositol 1,4,5-triphosphate receptor 1 during
766 in vitro maturation of porcine oocytes*. Anim. Sci. J.* **81**, 34-41 (2010).

767

768

769 **Figure legends**

770 **Fig. 1. Expression of ZIP6 and ZIP10 in mouse ovary. (**A) In situ hybridization
771 in the mouse ovary showed ZIP10 expression in oocyte and granulosa cell from
772 primordial, primary, secondary and antral follicle. (B) Immunofluorescent staining
773 for ZIP10 (green) in the mouse ovary showed ZIP10 expression in oocyte
774 membrane. Arrow indicates primordial follicular oocyte. (C) Immunofluorescent
775 staining for ZIP6 (green) in the mouse ovary showed ZIP6 expression in oocyte

776 nucleus and granulosa cells. Arrow indicates primordial follicular oocyte. (D)
777 Immunofluorescent staining showed ZP2 (green; zona pellucida) and FOXL2
778 (red; granulosa cells) in the mouse ovary. ZP2 was not stain in primordial follicle,
779 but primary, secondary and antral follicles stained. FOXL2 observed at granulosa
780 cells of all stage follicles. The scale bar represents 20 μm of primordial-secondary
781 follicle and 150 μm of antral follicle (A-D).
782
783 **Fig. 2 Number of collected oocytes and dynamics of zinc ion in *Zip10$^{d/d}$***
784 **mice.** (A) The results of average number of oocytes in each group. Data
785 represents the average ± SEM. These experiments were repeated at least thrice.
786 Statistical differences were calculated according to student *t*-test ($p > 0.05$; no
787 significant difference). (B) The percentage of extrusion of first polar body at 10,
788 12 and 14 h after IVM. These experiments were repeated at least thrice.
789 Statistical differences were calculated according to student *t*-test ($p > 0.05$; no
790 significant difference). (C) The morphology of spindle and chromosome
791 organization in *Zip10$^{f/f}$* and *Zip10$^{d/d}$* MII oocytes at 14 h after IVM. Anti–α-tubulin
792 antibody (green) was used to stain the spindles. Chromosomes were stained with
793 DAPI (blue). The scale bar represents 10 μm. (D) Comparison with the
794 fluorescence intensity of intracellular zinc ion in GV, MII and 2PN. The upper
795 images showed the fluorescence of intracellular zinc ion of oocyte or embryo
796 treated with FluoZin-3AM. Representative images are shown. The white dotted
797 circles indicate the positions of oocytes and embryos. Scale bars denote 10 μm.
798 The lower part showed the fluorescence intensity of zinc ions in oocytes or
799 embryos. Data represent the average ± SE of the experiments. For each
800 experiment, 10–20 oocytes/embryos were stained and used for the measurement
801 in each stage of the experiment, and these experiments were repeated three
802 times. Statistical differences were calculated according to the welch's *t*-test.
803 Different letters represent significant differences ($p < 0.05$).
804
805 **Fig. 3 Measurement of calcium spike and zinc spark in *Zip10$^{d/d}$* mice.** (A) The
806 representative images of before or after IVF in mouse oocytes. Left side images
807 showed before fertilization. Right side images showed after fertilization. The

808 oocytes increased calcium ion and released zinc ion shortly after fertilization. The
809 white dotted circles indicate the positions of oocytes. Successful fertilization was
810 confirmed by simultaneously monitoring intracellular calcium oscillations with
811 Calbryte 590 AM and excellular zinc ions with FluoZin-3 every 4 s. Capacitated
812 frozen-thawed sperm was added to ZP-free MII at 2 min after imaging start.
813 Orange line showed calcium ion and dark blue line showed zinc ion. Intracellular
814 calcium increases immediately before a zinc spark. (B) The representative
815 images of an MII egg activated with 5 μM ionomycin followed by monitoring of
816 intracellular calcium oscillations with Calbryte 590 AM and extracellular zinc using
817 20 μM FluoZin-3. The ionomycin was added to ZP-free MII at 2 min after imaging
818 start. Orange line showed calcium ion and dark blue line showed zinc ion.
819 Intracellular calcium increases immediately before a zinc spark.
820
821 **Fig. 4 Presence of a mechanism to prevent multisperm fertilization in Zip10**
822 **cKO mice.** (A) The percentages of oocytes with each number of PN at 6 h after
823 insemination. Yellow region showed other including degeneration, degression
824 and fragmentation. Gray region showed unfertilization, namely MII oocytes.
825 Orange showed 2PN2PB, namely embryo possessed one female and male
826 pronucleous (2PN) and second polar body (2PB). Blue region showed multisperm
827 fertilization (3PN2PB). (B) The percentage of fertilized oocytes and
828 developmental embryos. Data represent the average ± SE of the experiments.
829 These experiments were repeated at least thrice. Statistical differences were
830 calculated according to the chi-square test. Different letters represent significant
831 differences ($p < 0.05$). (C) The cell number of blastocyst derived from IVF.
832 Blastocysts were fixed, immunostained, and physically flattened between a slide
833 and coverslip. Photographs represent a single plane of focus. Nuclei are indicated
834 by DAPI staining. The count used inverted fluorescence microscope. These
835 experiments were repeated three times, and each group counted total 46
836 embryos. Statistical differences were calculated according to the student *t*-test (p
837 < 0.05; significant difference). (D) Western blot of oocytes from *Zip10*$^{f/f}$ and
838 *Zip10*$^{d/d}$ mice at 0 or 6 h after insemination using rat anti-ZP2 antibody. Intact ZP2
839 and the cleaved C-terminal fragment of ZP2 measured 120-130 kD and

840 undetected, respectively. Expression level of β-actin serves as a protein loading
841 control. Molecular mass is indicated at the left. (E) MII oocytes and 2PN embryos
842 from *Zip10*$^{f/f}$ and *Zip10*$^{d/d}$ mice were imaged by confocal microscopy after staining
843 with rabbit anti-ovastacin (green). Chromosomes were stained with DAPI (blue).
844 The scale bar represents 10 μm. (F) MII oocytes and 2PN embryos from *Zip10*$^{f/f}$
845 and *Zip10*$^{d/d}$ mice were imaged by BZ-X700 microscopy after staining with rat
846 anti-mouse FR4 (JUNO; green). Chromosomes were stained with DAPI (blue).
847 The scale bar represents 10 μm.
848
849 **Supplement Figure legends**
850
851 **Fig. S1 Generation of oocyte specific *Zip6* and *Zip10* conditional knockout**
852 **mouse.** (A) Schematic of mating pattern of *Zip6* and *Zip10* conditional knockout
853 mice. (B) Strategy used to develop floxed *Zip6* and *Zip10* allele. The mouse ZIP6
854 locus is shown at top. A loxP site (black triangle) sequence insert into a region
855 before and after exon 3 of *Zip6* to produce the *Zip6* floxed allele with loxP sites
856 flanking exons 3. In the presence of Cre recombinase there is further
857 recombination resulting in the inactivated *Zip6* allele lacking exons 3 (*Zip6* ∆flox).
858 The mouse ZIP10 locus is shown at top. A loxP site (black triangle) sequence
859 insert into a region between exons 5 and 6, and a loxP site sequence between
860 exons 8 and 9 of *Zip10* to produce the *Zip10* floxed allele with loxP sites flanking
861 exons 6-8. In the presence of Cre recombinase there is further recombination
862 resulting in the inactivated *Zip10* allele lacking exons 6-8 (*Zip10* ∆flox). (C)
863 Genotyping of flox, ∆flox and iCre was performed by genomic PCR. To elucidate
864 the roles of ZIP10 in the mouse oocytes, we crossed *Zip10*$^{flox/flox}$ (*Zip10*$^{f/f}$) mice
865 with Growth Differentiation factor 9 (*Gdf9*)-Cre transgenic mice to generate
866 *Zip10*$^{flox/flox}$ *Gdf9*-Cre (*Zip10*$^{d/d}$) mice. *Zip10*$^{f/f}$ mice were used as control. Similarly,
867 we crossed *Zip6*$^{flox/flox}$ (*Zip6*$^{f/f}$) mice with *Gdf9*-Cre transgenic mice to generate
868 *Zip6*$^{flox/flox}$ *Gdf9*-Cre (*Zip6*$^{d/d}$) mice. *Zip6*$^{f/f}$ mice were used as control. The tail tips
869 of 2 weeks old mice were cut. The samples were lysed in 100 μl of DirectPCR
870 Lysis Reagent (Viagen Biotech) with proteinase K (0.1 mg/ml) at 50°C for

871 overnight. To inactivate proteinase K, the samples were incubated at over 80 °C
872 for 1 h. The genotypes confirmed by polymerase chain reaction (PCR), as
873 suggested by Miyai et al., (2014) (62) and RIKEN BRC using
874 CAAGGCCAGCCAAAATTCTA (A-F) and GCTTTCCTCCCATCCTGATT (A-R)
875 to detect Wild-type (292 bp) and *Zip10* flox (420 bp), A-F and
876 GTGGCATGCGTGGAAGTTAG (B-R) to detected *Zip10* flox null (550 bp) alleles.
877 the genotyping of *Zip6* flox was confirmed using
878 CCAGCATTGCCCTCTGTAAGAGTC (*Slc39a6*_F) and
879 GCCTAAAGAAGATACACTGACACGACG (*Slc39a6*_R) to detect Wild-type (353
880 bp) and *Zip6* flox (387 bp), GGACCGGTTGCATAGAGGAG (*Slc39a6*_Null_F)
881 and GAGGCAGGCGGATTTCTGAG (*Slc39a6*_Null_R) to detected *Zip6* flox null
882 (500 bp) alleles. Similarly, we detected *Gdf9* iCre/+ alleles (200 bp) using
883 CAGGTTTTGGTGCACAGTCA (21218) and GGCATGCTTGAGGTCTGATTAC
884 (25494) to suggest by Jackson Laboratory. MII oocytes were used in order to
885 detect oocyte expression.
886
887 **Fig. S2 Number of collected oocytes, dynamics of zinc ion and percentage**
888 **of fertilization in *Zip6$^{d/d}$* mice.** (A) The results of average number of oocytes in
889 each group. Data represents the average ± SEM. These experiments were
890 repeated at least thrice. Statistical differences were calculated according to
891 student *t*-test ($p > 0.05$; no significant difference). (B) Comparison with the
892 fluorescence intensity of intracellular zinc ion in MII and 2PN. Data represent the
893 average ± SE of the experiments. For each experiment, 10–20 oocytes/embryos
894 were stained and used for the measurement in each stage of the experiment, and
895 these experiments were repeated three times. Statistical differences were
896 calculated according to student *t*-test ($p > 0.05$; no significant difference). (C) The
897 percentages of oocytes with each number of PN at 6 h after insemination. Yellow
898 region showed other including degeneration, degression and fragmentation. Gray
899 region showed unfertilization, namely MII oocytes. Orange showed 2PN2PB,
900 namely embryo possessed one female and male pronucleous (2PN) and second
901 polar body (2PB). Blue region showed multisperm fertilization (3PN2PB). (D) The
902 percentage of fertilized oocytes and developmental embryos. Data represent the

903 average ± SE of the experiments. These experiments were repeated at least
904 thrice. Statistical differences were calculated according to the chi-square test (p
905 > 0.05).
906
907 **Fig. S3 Measurement of calcium spike and zinc spark in *Zip6*$^{d/d}$ mice.** The
908 representative images of before or after IVF in mouse oocytes. Left side images
909 showed before fertilization. Right side images showed after fertilization. The
910 oocytes increased calcium ion and released zinc ion shortly after fertilization. The
911 white dotted circles indicate the positions of oocytes. Successful fertilization was
912 confirmed by simultaneously monitoring intracellular calcium oscillations with
913 Calbryte 590 AM and excellular zinc ions with FluoZin-3 every 4 s. Capacitated
914 frozen-thawed sperm was added to ZP-free MII at 2 min after imaging start.
915 Orange line showed calcium ion and dark blue line showed zinc ion. Intracellular
916 calcium increases immediately before a zinc spark.
917
918
919
920
921
922
923
924
925
926
927
928
929
930
931
932

933
934
935
936
937 **Fig. 1**
938
939 Primordial follicle | Primary follicle | Secondary follicle | Antral follicle
940 A
941 *Zip10* mRNA
942
943
944 B
945 ZIP10/*Slc39a10*
946
947
948 C
949 ZIP6/*Slc39a6*
950
951
952
953 D
954 ZP2
955 FOXL2
956
957
958
959
960

Fig. 2

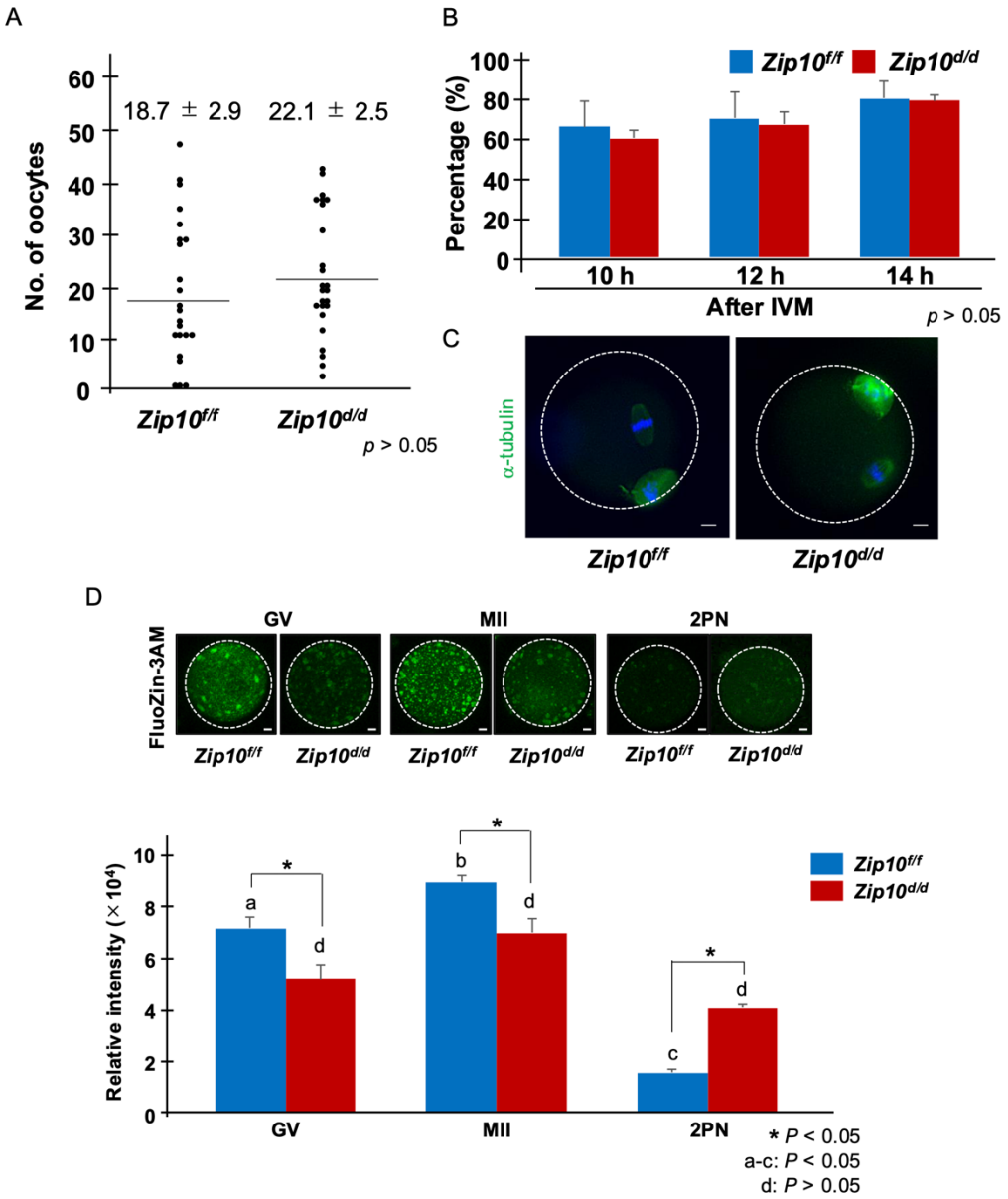
A
No. of oocytes
18.7 ± 2.9
22.1 ± 2.5
Zip10f/f
Zip10d/d
p > 0.05
B
Percentage (%)
Zip10f/f
Zip10d/d
10 h
12 h
14 h
After IVM
p > 0.05
C
α-tubulin
Zip10f/f
Zip10d/d
D
FluoZin-3AM
GV
MII
2PN
Zip10f/f
Zip10d/d
Relative intensity (×10⁴)
a
d
b
d
c
d
*
* P < 0.05
a-c: P < 0.05
d: P > 0.05

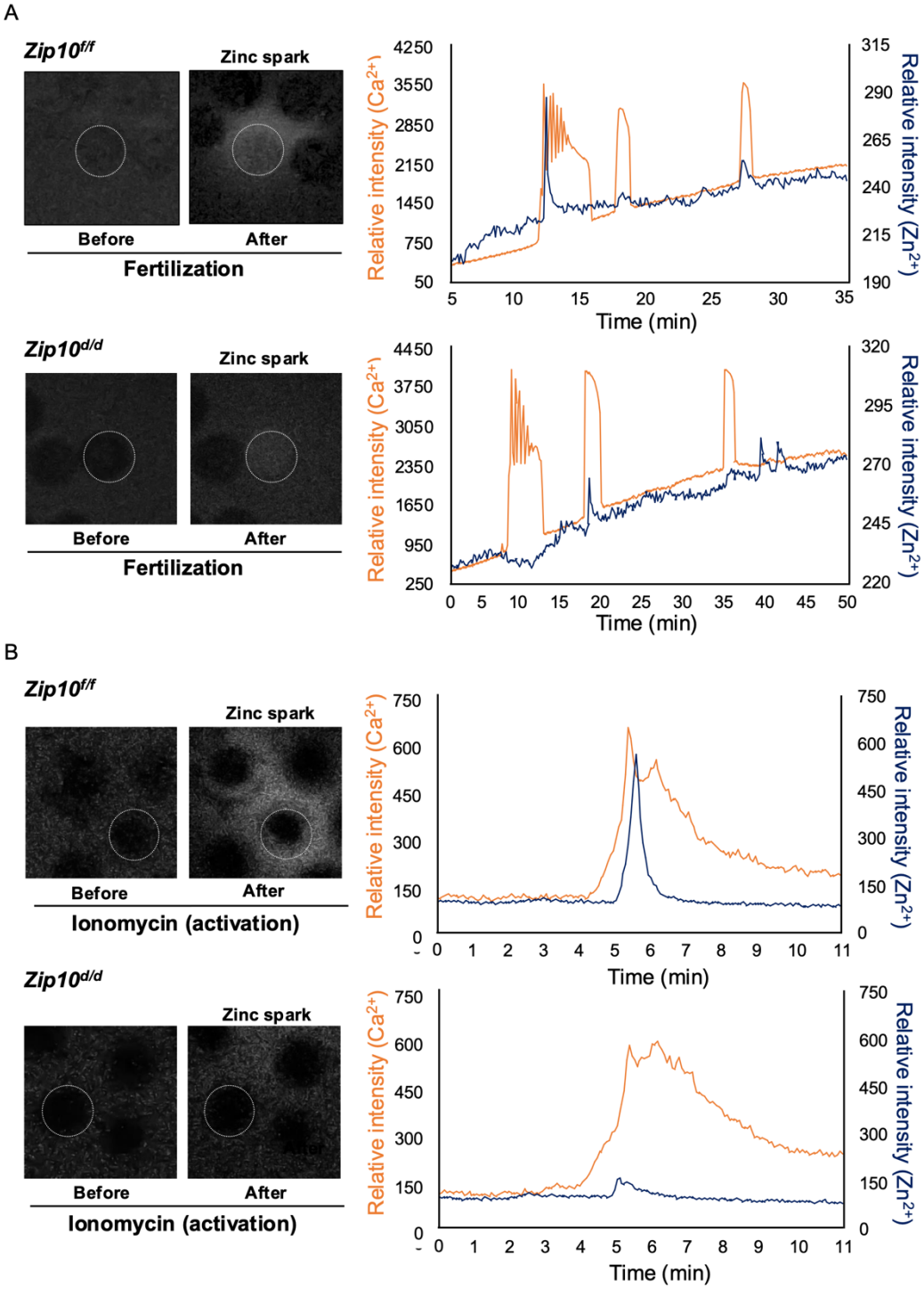
A
Zip10f/f
Zinc spark
Before
After
Fertilization
Relative intensity (Ca2+)
Relative intensity (Zn2+)
Time (min)
Zip10d/d
Zinc spark
Before
After
Fertilization
Relative intensity (Ca2+)
Relative intensity (Zn2+)
Time (min)
B
Zip10f/f
Zinc spark
Before
After
Ionomycin (activation)
Relative intensity (Ca2+)
Relative intensity (Zn2+)
Time (min)
Zip10d/d
Zinc spark
Before
After
Ionomycin (activation)
Relative intensity (Ca2+)
Relative intensity (Zn2+)
Time (min)

1017

1018

1019

1020 **Fig. 4**

1021

1022

1023

1024

1025

1026

1027

1028

1029

1030

1031

1032

1033

1034

1035
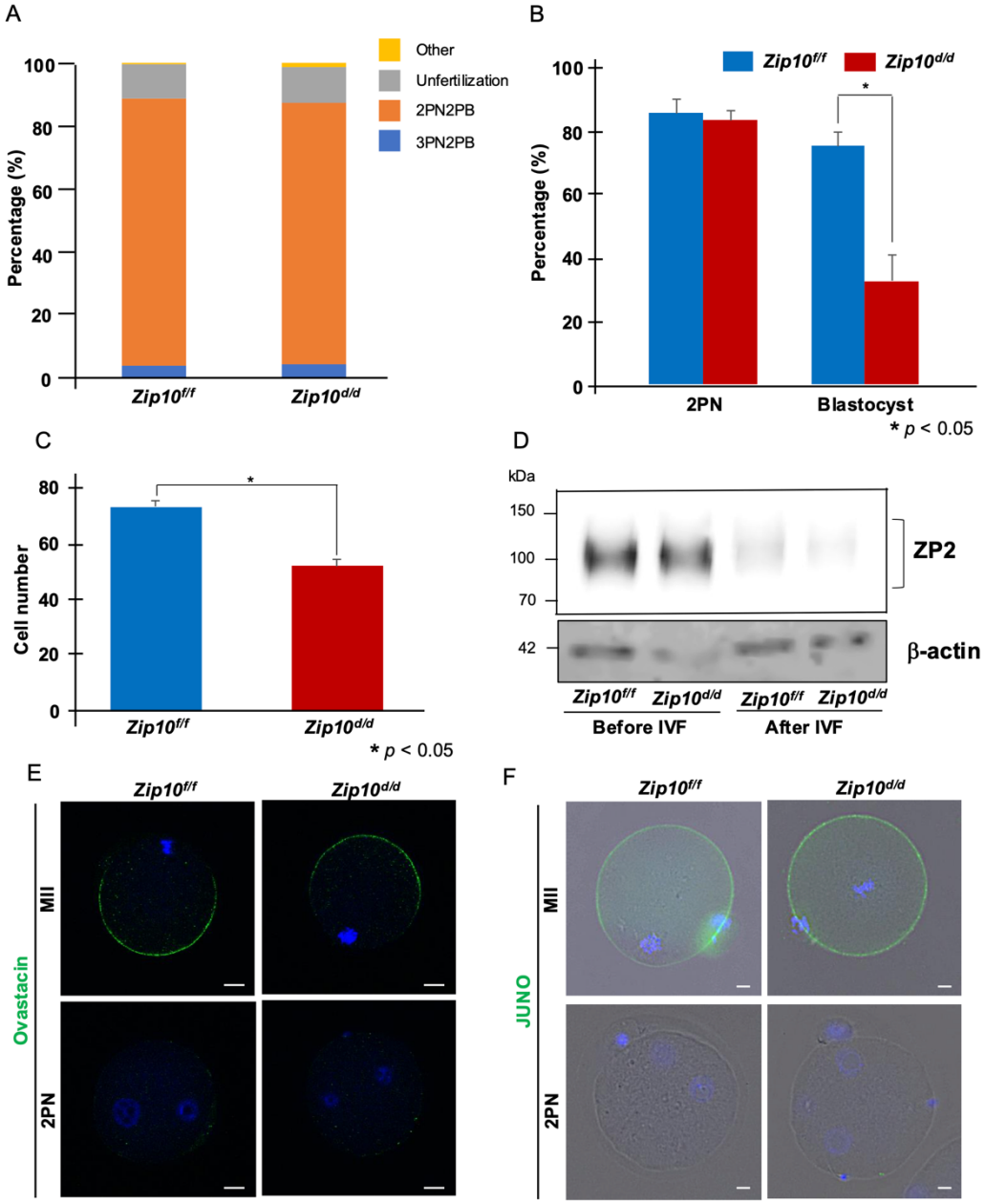
1036